IVYSPRING INTERNATIONAL PUBLISHER

Theranostics

2016; 6(5): 627-637. doi: 10.7150/thno.14792

Research Paper

Enhanced Anti-Tumor Efficacy through a Combination of Integrin αvβ6-Targeted Photodynamic Therapy and Immune Checkpoint Inhibition

Liquan Gao[1], Chenran Zhang[1], Duo Gao[1], Hao Liu[1], Xinhe Yu[1], Jianhao Lai[1], Fan Wang[1], Jian Lin[2], Zhaofei Liu[1]✉

1. Medical Isotopes Research Center and Department of Radiation Medicine, School of Basic Medical Sciences, Peking University Health Science Center, Beijing 100191, China;
2. Synthetic and Functional Biomolecules Center, College of Chemistry and Molecular Engineering, Peking University, Beijing 100871, China.

✉ Corresponding author: Zhaofei Liu, Ph.D., Medical Isotopes Research Center and Department of Radiation Medicine, School of Basic Medical Sciences, Peking University Health Science Center, Beijing 100191, China. Phone: +86-1082802871; Fax: +86-1082802871; E-mail: liuzf@bjmu.edu.cn.

Received: 2015.12.23; Accepted: 2016.01.27; Published: 2016.03.03

Abstract

"Training" the host immune system to recognize and systemically eliminate residual tumor lesions and micrometastases is a promising strategy for cancer therapy. In this study, we investigated whether integrin αvβ6-targeted photodynamic therapy (PDT) of tumors using a phthalocyanine dye-labeled probe (termed DSAB-HK) could trigger the host immune response, and whether PDT in combination with anti-PD-1 immune checkpoint inhibition could be used for the effective therapy of primary tumors and metastases. By near-infrared fluorescence imaging, DSAB-HK was demonstrated to specifically target either subcutaneous tumors in a 4T1 mouse breast cancer model or firefly luciferase stably transfected 4T1 (4T1-fLuc) lung metastatic tumors. Upon light irradiation, PDT by DSAB-HK significantly inhibited the growth of subcutaneous 4T1 tumors, and in addition promoted the maturation of dendritic cells and their production of cytokines, which subsequently stimulated the tumor recruitment of $CD8^+$ cytotoxic T lymphocytes. Furthermore, DSAB-HK PDT of the first tumor followed by PD-1 blockade markedly suppressed the growth of a second subcutaneous tumor, and also slowed the growth of 4T1-fLuc lung metastasis as demonstrated by serial bioluminescence imaging. Together, our results demonstrated the synergistic effect of tumor-targeted PDT and immune checkpoint inhibition for improving anti-tumor immunity and suppressing tumor growth/metastasis.

Key words: Molecular imaging; Photodynamic therapy; Checkpoint inhibition; Tumor metastasis; Combination therapy.

Introduction

Cancer remains one of the leading causes of death worldwide, and cancer-related deaths, over 90% of which currently result from metastatic disease and its related complications, have been estimated to reach 11.5 million by the year 2030 [1-3]. Notably, by the time that cancer is detected in most patients, metastases may have already occurred that are either apparent at the site of major organs or represent clinically occult micro-metastases [4]. In clinical practice, the primary tumor and a small number of cancer metastases with large and well-vascularized patterns might be cured by surgical intervention; however, strategies for the effective treatment of local or long distant metastasis and especially of micro-metastases are generally limited. As these micro-metastases or small clusters of disseminated malignant cells usually cause tumor relapse and eventual treatment failure, systemic treatment strategies or combination strategies that effectively treat both primary tumor and metastatic lesions are greatly needed for the effective

cure of cancer.

Cancer immunotherapy, which induces anti-tumor immunity by "educating" the host immune system to recognize and systemically eliminate any remaining tumor lesions (both primary and metastatic) by prompt surveillance and defense, has been expected to be a promising approach for effective cancer management [5, 6]. T lymphocyte activation, especially cytotoxic $CD8^+$ T effector cells, during cancer immunotherapy in particular plays an important role in inhibiting and killing tumor cells. However, it is generally difficult for the host to generate sufficient immune responses to effectively eradicate all cancer. Cancer can evade host immune surveillance through a process of T lymphocyte exhaustion, which results in the expression of inhibitory receptors that trigger immune checkpoints and are critical for maintaining self-tolerance [7, 8]. To overcome this, checkpoint inhibitors (e.g., monoclonal antibodies that are able to block these inhibitory receptors) are being extensively investigated as novel cancer therapeutics with great potential to augment anti-tumor immunity. Of these, antibody-based blockade of cytotoxic T-lymphocyte-associated protein 4 (CTLA-4) and programmed death-1 (PD-1) are the most studied strategies for immune checkpoint inhibition [8]. The anti-CTLA-4 antibody ipilimumab has been approved by the FDA for melanoma therapy, and has demonstrated enhanced overall survival compared with standard care [9, 10]. In addition, several antibodies against PD-1 such as nivolumab have also demonstrated encouraging anti-tumor effects in multiple clinical trials [11, 12].

Photodynamic therapy (PDT) is a cancer phototherapy approach that employs a combination of light, a photosensitizer, and oxygen to destroy cancer cells by generating cytotoxic reactive oxygen species, especially singlet oxygen. The near-infrared fluorescence (NIRF) phthalocyanine dye IRDye700 can serve as a photosensitizer for potential cancer PDT; as this dye has emission wavelengths in the 700~900 nm range, in which tissue autofluorescence is minimal, it allows for favorable tissue penetration for potential in vivo imaging [13]. The use of IRDye700-labeled monoclonal antibodies has been well established as a powerful approach to image and locate primary and metastatic tumors and also to treat a wide variety cancers in animal models [14-17]. In our recent study, we developed an IRDye700-coupled NIRF probe, IRDye700-streptavidin-biotin-HK peptide (DSAB-HK; **Figure S1**), which can be used for the diagnostic imaging and therapy of tumors by specific targeting of integrin αvβ6, an integrin family member that is overexpressed in a variety of cancer types [18], through the HK peptide.

In addition to direct effects on tumor cells through either necrosis and/or apoptosis, PDT has also been reported to have an indirect effect by stimulating the host immune system [19, 20]. PDT-induced cancer cell death causes acute inflammation, which might augment immunity by increasing antigen presentation and forming more effective tumor-specific cytotoxic T lymphocytes [20]. In this study, we investigated whether integrin αvβ6-targeted PDT of tumors via DSAB-HK could activate a tumor-specific immune response, and whether PDT in combination with anti-PD-1 immune checkpoint inhibition could facilitate primary tumor eradication as well as eliminating the metastatic lesions.

Materials and Methods

Materials

All commercially obtained chemicals were of analytical grade and used without further purification. The peptide RGDLATLRQLAQEDGVVGVRK (HK peptide; **Figure S1**) was custom synthesized by ChinaPeptides Co., Ltd (Shanghai, China). $Na^{125}I$ was purchased from Perkin-Elmer (Waltham, MA). Female BALB/c mice (4~5 weeks of age) were obtained from Department of Laboratory Animal Science, Peking University (Beijing, China).

DSAB-HK and IRDye700-streptavidin-biotin (DSAB) preparation

The integrin αvβ6-specific near-infrared phthalocyanine dye-labeled agent DSAB-HK and the control agent DSAB were synthesized by using streptavidin-biotin chemistry as previously described [18].

^{125}I-SAB-HK and ^{125}I-SAB preparation

Streptavidin was radiolabeled with $Na^{125}I$ using a previously describe method [21]. After labeling ^{125}I-streptavidin (^{125}I-SA) was purified using a PD-10 desalting column (GE Healthcare, Piscataway, NJ). ^{125}I-SA was mixed with excess amounts of biotin-HK (B-HK) or biotin only, and then the unbound B-HK or biotin was removed using a PD-10 desalting column. The resulting ^{125}I-SAB-HK and ^{125}I-SAB were concentrated using a Centricon filter (Millipore, Bedford, MA).

Cell culture and animal models

The 4T1 murine breast cancer cell line was obtained from the American Type Culture Collection. Firefly luciferase stably transfected 4T1 (4T1-fLuc) cells were generated using a previously described method [22]. Cells were maintained in RPMI 1640 medium (Invitrogen, Carlsbad, CA) supplemented with 10% fetal bovine serum (FBS) at 37°C in humidi-

fied atmosphere containing 5% CO_2.

All animal experiments were performed in accordance with the Guidelines of the Peking University Animal Care and Use Committee. To establish the 4T1 subcutaneous tumor model, 1×10^6 4T1 tumor cells were inoculated subcutaneously into the right hind legs of BALB/c mice. For the second tumor challenge studies, mice were injected subcutaneously with 1×10^6 4T1 tumor cells into the left hind legs, and six days later with 2×10^5 tumor cells into the right hind legs. For the lung metastatic tumor model, 5×10^5 4T1-fLuc cells were injected via tail vein into BALB/c mice. For the dual subcutaneous and lung metastatic tumor model, 4×10^5 4T1-fLuc tumor cells were inoculated subcutaneously into the right hind legs and 5×10^4 4T1-fLuc tumor cells were injected into the mice through the tail vein. The growth of subcutaneous tumors was measured using a caliper, and the tumor volume was calculated using the following formula: tumor volume = length × (width^2)/2.

In vivo NIRF imaging

4T1 tumor-bearing mice (n = 5 per group) were injected with 0.5 nmol DSAB-HK or DSAB with or without a blocking dose (300 μg) of HK peptide through the tail vein. At 1, 2, 4, 8, and 24 h after injection, mice were anesthetized by inhalation of 2% isoflurane in oxygen and then optical imaging was performed using an IVIS small-animal imaging system (Xenogen, Alameda, CA). The tumor uptake of DSAB-HK or DSAB was determined by normalizing the fluorescence intensity of the tumor by the injection dose as previously described [23].

Small-animal single-photon emission computed tomography (SPECT)/CT

4T1 tumor-bearing mice (n = 3 per group) were injected via tail vein with 18.5 MBq ^{125}I-SAB-HK or ^{125}I-SAB. For the blocking experiment, three 4T1 tumor-bearing mice were coinjected with 300 μg HK peptide and 18.5 MBq ^{125}I-SAB-HK. At 24 h postinjection, mice were anesthetized by inhalation of 2% isoflurane in oxygen and small-animal SPECT/CT scans were performed on a NanoScan SPECT/CT imaging system (Mediso, Budapest, Hungary) as previously described [22]. The tumor uptake of ^{125}I-SAB-HK or ^{125}I-SAB was quantified using a previously described method [24].

In vivo PDT-triggered immunological responses

4T1 tumor-bearing mice were segregated into 6 groups: phosphate-buffered saline (PBS) control, light only, DSAB, DSAB-HK, DSAB PDT, and DSAB-HK PDT groups (n = 12 per group). Mice were injected via tail vein with PBS, 1 nmol DSAB, or 1 nmol DSAB-HK on days 0, 1, and 2. Light irradiation (70 J/cm^2) was performed on the tumors using a 690-nm laser (Shanghai Laser & Optics Century Co., Ltd., Shanghai, China) for the light only, DSAB PDT, and DSAB-HK PDT group at 4 h postinjection of PBS, DSAB, or DSAB-HK. Tumor sizes were measured every other day.

On day 9, five mice from each group were sacrificed, and serum samples and tumor-draining lymph nodes (TDLNs) were collected for enzyme-linked immunosorbent assay (ELISA) and flow cytometric analysis, respectively. For the serum samples, ELISA analysis of interleukin (IL)-1β and IL-12P70 was performed using ELISA kits (eBioscience, San Diego, CA) following the manufactures' instructions. For the TDLN samples, single-cell suspensions were obtained by digestion with 10 U/mL collagenase I, 400 U/mL collagenase IV, and 30 U/mL DNase (in PBS) for 1 h at 37°C, and then passed through a 70-μm cell strainer. Cells were stained with anti-CD11c (FITC) and anti-CD83 (PE) antibodies (eBioscience), and then sorted using an LSR-II flow cytometer (Becton Dickinson, Germany).

Tumor challenge experiments

4T1 tumor-bearing mice were segregated into 4 groups (n = 20~25 per group): control, DSAB-HK PDT, anti-PD-1, and DSAB-HK PDT + anti-PD-1. Mice were injected with PBS or 1 nmol DSAB-HK daily for 3 days (from day -3 to day -1). The first tumors were irradiated at 70 J/cm^2 by light using the 690-nm laser at 4 h postinjection of DSAB-HK. After treatment, the first tumors were removed by surgery (on day 0), and mice in the anti-PD-1 groups were treated by intravenous injection of 100 μg anti-PD-1 antibody (BioXcell, West Lebanon, NH) [25] every other day for 3 days (on days 1, 3, and 5). The growth of the second tumors of the mice was measured every other day. Mice were euthanized when the tumor size exceeded the volume of 1500 mm^3. On day 12, five mice from each group were examined for lung metastasis as described below. Another five mice from each group were sacrificed, and tumors were harvested. Half of each tumor sample was immediately frozen in OCT medium can then cut into 5-μm-thick slices for immunofluorescence staining of CD8. The other half of each tumor was digested to obtain single-cell suspensions. After staining with anti-CD4 (APC) and anti-CD8 (PE) antibodies (eBioscience), cells were sorted using the LSR-II flow cytometer.

Immunofluorescence staining

After blocking with 10% FBS (in PBS), the tumor slices were incubated with anti-CD8α (eBioscience)

primary antibody for 1 h at room temperature and then visualized with a dye-conjugated secondary antibody under a Leica TCS-NT confocal microscope (Wetzler, Heidelberg, Germany).

Lung metastasis examination

The mice were scanned by computed tomography (CT) focusing on the chests using the NanoScan SPECT/CT imaging system. Afterwards, the lungs of mice were filled with 15% India ink via the upper trachea and then fixed as previously described [26]. Tumor metastatic lesions on the lung surface were counted. Lungs were then embedded in paraffin, and hematoxylin and eosin (H&E) staining was performed.

In vivo targeting of DSAB-HK in lung metastases

To target lung metastasis, 0.5 nmol DSAB-HK or DSAB was intravenously injected into 4T1-fLuc lung metastatic mice or normal BALB/c mice (n = 5 per group). At 1, 2, 4, and 8 h postinjection, mice were subjected to NIRF imaging using an IVIS small-animal imaging system. For bioluminescence imaging (BLI), mice received an intraperitoneal injection of 150 mg/kg D-luciferin (Gold BioTechnology, St Louis, MO), and then BLI was performed using the IVIS spectrum system 10 min after D-luciferin administration. After BLI, mice were sacrificed, and the lungs were harvested, placed on a black paper, and then scanned by NIRF imaging to determine the location of DSAB-HK or DSAB.

Following the last NIRF scan at 8 h postinjection, mice were sacrificed and the major organs/tissues of mice were dissected, weighed, and NIRF imaged ex vivo. The organ uptake of DSAB-HK and DSAB were calculated as the percent injected dose per gram (%ID/g) as previously described [26].

Combination therapy

The DSAB-HK and anti-PD-1 combination study was performed in the dual subcutaneous and lung metastatic 4T1-fLuc tumor model. Mice were treated with DSAB-HK PDT on days 1 and 5 by i.v injection of 2 nmol DSAB-HK followed by light irradiation of the subcutaneous tumor or both the subcutaneous tumor and the chest at 35 J/cm^2 at 4 h postinjection. In the combination therapy groups, mice were injected via the tail vein with three doses of anti-PD-1 antibody (100 μg per mouse) immunotherapy on days 2, 6, and 8. Baseline and longitudinal BLI were performed to evaluate the growth of lung metastatic lesions. BLI was performed using the IVIS spectrum system 10 min after D-luciferin administration. The BLI signal intensity was quantified as the sum of all detected photon counts within the region of interest after subtraction of the background luminescence.

At the end of the combination study (day 11), the mice were sacrificed. The lungs of five mice from each group were filled with India ink and fixed. Lung metastatic lesions were counted as described above. Another five mice from each group were directly sacrificed, and the lungs were harvested and weighed.

Statistical analysis

Data were are presented as mean ± SD. Statistical analysis was done using a 1-way ANOVA and an unpaired Student's *t* test. *P* values <0.05 were considered statistically significant.

Results and Discussion

In vivo specific tumor targeting of DSAB-HK

The integrin αvβ6-specific NIRF probe IRDye700-streptavidin-biotin-HK peptide (DSAB-HK; **Figure S1**) was prepared by mixing IRDye700-labeled streptavidin with biotin-conjugated HK peptide (integrin αvβ6-specific) [27]. Before testing its in vivo applications for tumor targeting, we first characterized the probe in vitro. By singlet oxygen sensor green assay, we confirmed the singlet oxygen generation of DSAB-HK (**Figure S2**), suggesting its PDT potential. We next investigated the integrin αvβ6 expression of 4T1 tumor cells, which were used in this study to generate the in vivo animal models. By immunofluorescence staining, specific integrin β6 staining was observed for the 4T1 cells (**Figure S3**). With respect to integrin heterodimers (α and β subunits), the β6 subunit only combines with αv to generate a single heterodimer [28], therefore, our immunofluorescence study confirmed the expression of integrin αvβ6 on the 4T1 tumor cells. We then detected the integrin αvβ6-specific PDT effect of DSAB-HK in vitro. Compared with DSAB, which represents a negative control without the HK targeting peptide, a significant irradiation dose-dependent toxicity was observed for DSAB-HK in the 4T1 tumor cells (**Figure S4**), demonstrating the receptor-specific PDT effect of DSAB-HK.

We next investigated the in vivo tumor targeting of DSAB-HK in 4T1 tumor-bearing mice, and DSAB was used as a control. The 4T1 tumors could be clearly visualized by NIRF imaging of DSAB-HK with high contrast in relation to the contralateral background at all time points measured from 1 to 24 h (**Figure 1 A** and **Figure S5**). The tumor uptake of DSAB-HK was significantly higher than that of the DSAB (e.g., 5.24 ± 0.44 % vs. 3.98 ± 0.48 % at 4 h postinjection.; $P < 0.01$; **Figure 1A** and **B**), suggesting the specific delivery of DSAB-HK in the tumor by the HK targeting. The integrin αvβ6 binding specificity of DSAB-HK in vivo was also confirmed by blocking studies, wherein the tumor uptake of DSAB-HK was significantly inhibited

by coinjection of an excess dose of HK peptide (e.g., 3.41 ± 0.25 % vs. 1.31 ± 0.36 % at 24 h postinjection; $P < 0.001$; **Figure 1A** and **C**). Ex vivo organ distribution of the probes further validated the in vivo results (**Figure S6**). Notably, the tumor uptake of DSAB-HK with HK peptide blocking was significantly lower than that of the DSAB conjugate without the HK peptide (**Figure 1B, C**). A possible explanation for this phenomenon is that coinjecting with an excess dose of unlabeled HK peptide affected the in vivo pharmacokinetics of DSAB-HK by accelerating its clearance from the circulation and the tumor itself.

Optical imaging has limitations of data quantification owing to the limited photon penetration of tissue and intra-tissue light scattering. We thus prepared a radio-counterpart of DSAB-HK, ^{125}I-SAB-HK, by radiolabeling streptavidin with Na^{125}I, and then connecting ^{125}I-SA with B-HK. The in vivo distribution of ^{125}I-SAB-HK was evaluated by high resolution and high sensitive small-animal SPECT/CT imaging. **Figure 1D** shows the representative SPECT/CT images of ^{125}I-SAB-HK or ^{125}I-SAB with or without the presence of unlabeled HK blocking at 24 h postinjection. The tumor was clearly visualized by SPECT/CT imaging of ^{125}I-SAB-HK. Although deiodination occurred for both ^{125}I-SAB-HK and ^{125}I-SAB as evidenced by high accumulation of activity in the mouse thyroids, a significantly higher tumor uptake was observed for ^{125}I-SAB-HK as compared to that of ^{125}I-SAB ($P < 0.01$; **Figure 1E**) and ^{125}I-SAB-HK (unlabeled HK blocking; $P < 0.001$; **Figure 1E**). These results further indicated the tumor-specific localization of DSAB-HK to the 4T1 tumor.

In vivo PDT of DSAB-HK in 4T1 tumors prompts the maturation of dendritic cells

The specific localization of DSAB-HK to the 4T1 tumor suggests that upon light irradiation, DSAB-HK might have an anti-tumor effect based on PDT. We therefore evaluated the PDT effect of DSAB-HK in the subcutaneous 4T1 tumor model. Compared with the PBS control group, the light only, DSAB only, DSAB + light irradiation (DSAB PDT), and DSAB-HK only treatments had no effect on the inhibition of tumor growth. In contrast, a significant delay in tumor growth was observed in the DSAB-HK PDT group after three doses of therapy (**Figure 2A**). However, compared with the results of DSAB-HK PDT in the BxPC-3 tumor model as we had previously determined [18], the anti-tumor effect of DSAB-HK PDT in the 4T1 tumor model was lower. Specifically, DSAB-HK PDT could not fully inhibit the growth of 4T1 tumors in vivo, which is possibly due to the much more aggressive characteristics of the 4T1 tumor cells compared to BxPC-3 cells.

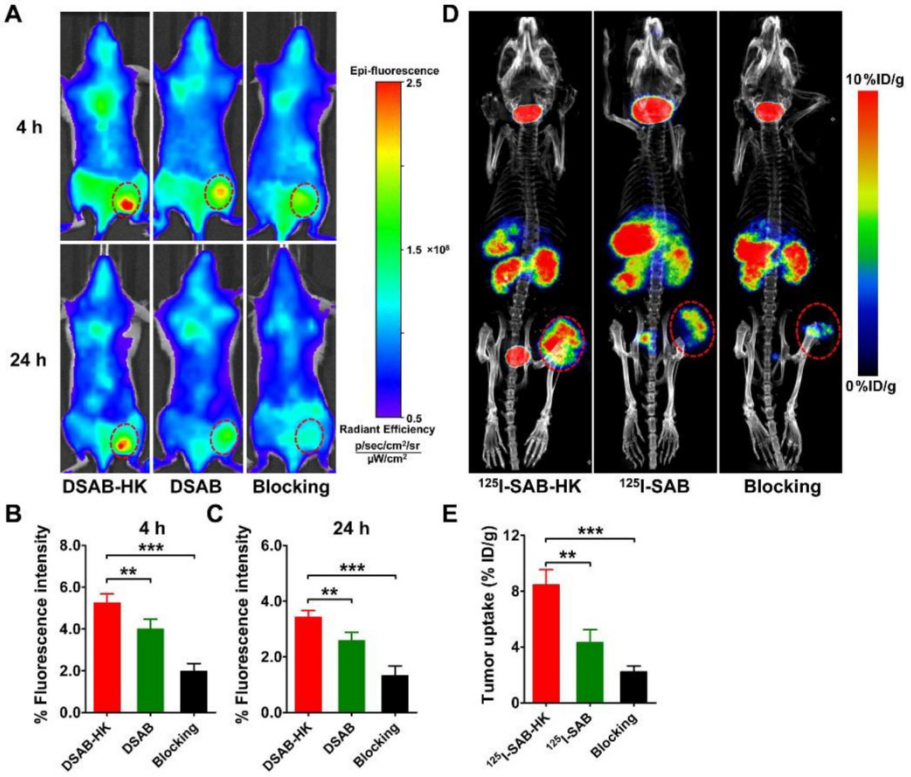

Figure 1. In vivo tumor-specific targeting of DSAB-HK in the subcutaneous 4T1 mouse model. (A) In vivo NIRF imaging of 4T1 tumor-bearing mice at 4 and 24 h after injection of DSAB-HK (with or without a blocking dose of HK peptide) or DSAB. (B, C) Quantified 4T1 tumor uptake of DSAB-HK (with or without a blocking dose of HK peptide) or DSAB at 4 (B) and 24 (C) h after injection. (D, E) Small-animal SPECT/CT imaging (D) and quantified tumor uptake (E) of 4T1 tumor-bearing mice at 24 h after injection of ^{125}I-SAB-HK (with or without a blocking dose of HK peptide) or ^{125}I-SAB. Tumors are indicated with circles. **, $P < 0.01$; ***, $P < 0.001$.

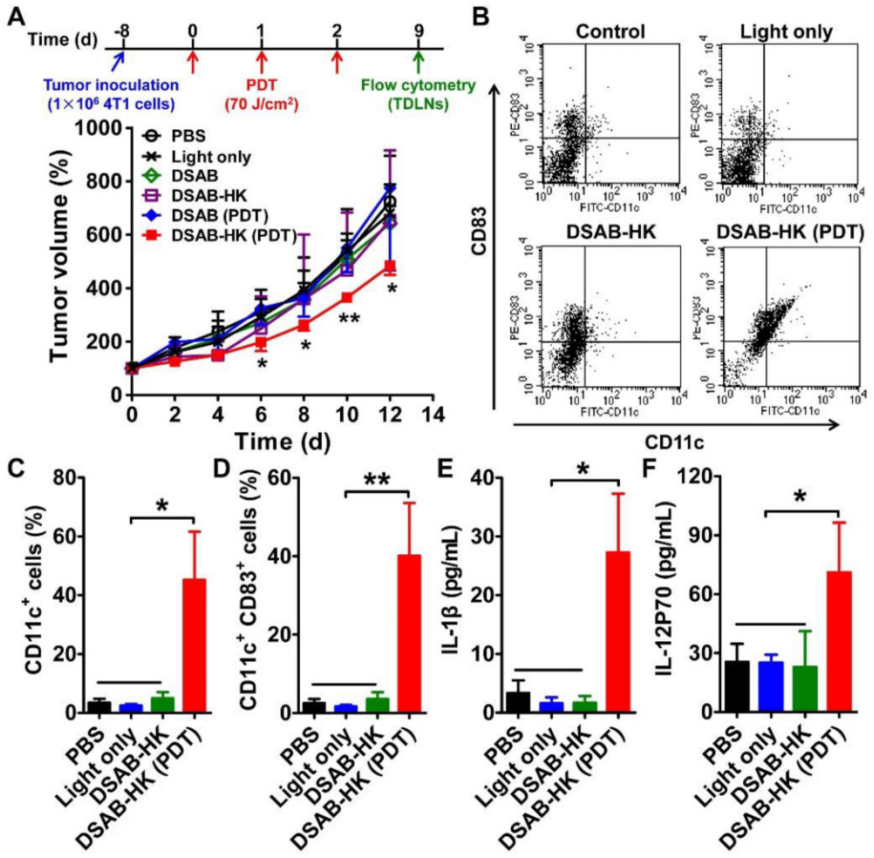

Figure 2. DSAB-HK PDT inhibition of 4T1 tumor growth and promotion of DC recruitment and maturation in TDLN. (A) 4T1 tumor growth curves of mice after various treatments. Inset, scheme of DSAB-HK PDT. (B-D) Representative dot plots (B), and $CD11c^+$ (C) and $CD11c^+CD83^+$ (D) cells quantified by flow cytometric analyses of CD11c and CD83 expression in the TDLN single-cell suspension harvested from mice after the different treatments as indicated. (E, F) Cytokine levels in the serum from mice after different treatments as measured by ELISA. *, $P < 0.05$; **, $P < 0.01$.

Although DSAB-HK PDT cannot entirely inhibit the growth of 4T1 tumors in the subcutaneous model, we observed a significant recruitment and maturation of dendritic cells (DCs) in the TDLN as indicated by significantly enhanced $CD11c^+$ ($P < 0.05$; **Figure 2B** and **C**) and $CD11c^+CD83^+$ ($P < 0.01$; **Figure 2B** and **D**) cell populations in the tumors of the DSAB-HK PDT group. DCs are professional antigen-presenting cells, which enable the presentation of antigen to $CD8^+$ cytotoxic T lymphocytes [20]. Therefore, the recruitment and maturation of DCs after PDT were most likely occurred because of stimulation from the antigen released by the PDT-killed tumor cells. To further validate the maturation of DCs after DSAB-HK PDT, we performed ELISA to determine the serum levels of IL-1β and IL-12, which are both produced by DCs upon antigen stimulation [29, 30]. Our results showed a significant upregulation of IL-1β and IL-12 (P70) levels in the DSAB-HK PDT group compared with the control groups ($P < 0.05$; **Figure 2E** and **F**), confirming the accumulation and maturation of DCs triggered by PDT.

Synergistic effect of DSAB-HK PDT and PD-1 blockade

As recent studies have demonstrated the enhanced anti-tumor immunity following tumor cryoablation, photothermal therapy, and radiation therapy in combination with immune checkpoint inhibition [31-33], we next determined the synergistic effect of DSAB-HK PDT and PD-1 blockade in a subsequent tumor challenge model. We inoculated 4T1 tumor cells into the left hind legs of BABL/c mice, and six days later the mice were challenged with a second injection of 4T1 tumor cells (**Figure 3A**). After 3 treatments with DSAB-HK PDT on the first tumor, the first tumors were removed by surgery, and mice were treated by intravenous injection of three doses of anti-PD-1 monoclonal antibody (100 μg daily for 3 days on days 1, 3, and 5), and the growth and lung metastasis of the second tumors were monitored. Compared with the control, PDT only, and PD-1 blockade groups, DSAB-HK PDT followed by PD-1 blockade significantly slowed the growth of the second tumors (**Figure 3B**). In addition, PD-1 blockade only or DSAB-HK PDT only did not have any evident effect on mouse survival. In contrast, DSAB-HK PDT followed by PD-1 blockade caused a significant extension of survival (38 d compared with 26 d for the control groups; $P < 0.05$; **Figure 3C**).

We then assessed the anti-metastatic effect of

combination therapy by examining the lung metastasis of the second 4T1 tumors. Markedly gray regions were observed in the lung areas of mice in the control, PDT only, and PD-1 blockade only groups. In contrast, a much clearer lung imaging was observed for the combination treatment group (**Figure 3D**). To validate the noninvasive CT imaging results, we harvested the lungs immediately after CT scanning and filled them with India ink, which causes the metastatic lesions to appear as white nodules on a black lung. A large number of metastatic lesions were observed in the lungs of control mice, PDT, and anti-PD-1 groups on day 12 as revealed by gross observation (**Figure 3E**) and H&E staining (**Figure 3F**). In contrast, a significantly smaller number of pulmonary metastases was observed for the combination therapy group ($P < 0.01$; **Figure 3G**). These results demonstrated that the PD-1 blockade remarkably increased the anti-tumor growth and metastasis effects of PDT.

To analyze the underlying mechanisms for the enhanced anti-tumor effect of the combination therapy, we investigated whether PD-1 blockade could enhance cytotoxic T lymphocyte infiltration following dendritic cell antigen presentation after PDT treatment. T lymphocyte infiltration was assessed 16 days later after the second tumor inoculation. Tumor cells harvested from mice after different treatments were sorted by flow cytometry using anti-CD4 and anti-CD8 antibodies to determine the types of T lymphocytes that had infiltrated the tumor. After sorting, we found that all groups contained similar patterns of $CD4^+$ T lymphocyte infiltration. However, a notably increased percentage of $CD8^+$ T lymphocytes within the second tumor was observed when mice were treated with DSAB-HK PDT + PD-1 blockade (**Figure 4A** and **B**). We further stained the second tumors with an anti-CD8α antibody, and found that the DSAB-HK PDT + PD-1 blockade combination-treated tumors were highly infiltrated with $CD8^+$ T lymphocytes (**Figure 4C**), which is consistent with the flow cytometric results.

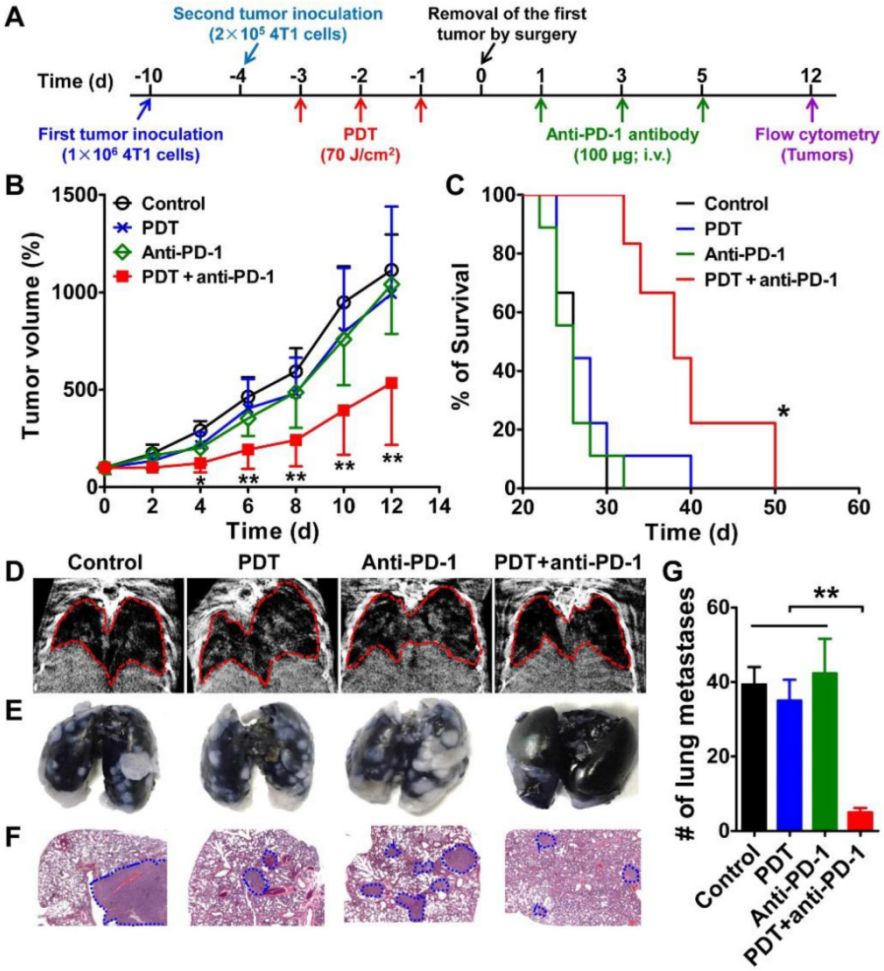

Figure 3. Inhibition of the growth and metastasis of the second tumor in mice treated with DSAB-HK PDT of the first tumor followed by PD-1 blockade. (A) Scheme of DSAB-HK PDT and PD-1 blockade combination therapy. (B, C) Growth curves the second 4T1 tumors in mice (B) and mouse survival curves (C) after different treatments of the first tumor and then removal the first tumor by surgery. (D-G) Representative images of in vivo CT scanning (D), India ink-filled lungs (E), H&E-stained lung sections (F), and the counted averages of tumor metastatic lesions in the lungs (G) from mice after the indicated treatments. Lungs in the CT images and tumor metastases in the H&E-stained lung slices are indicated by dashed circles. *, $P < 0.05$; **, $P < 0.01$.

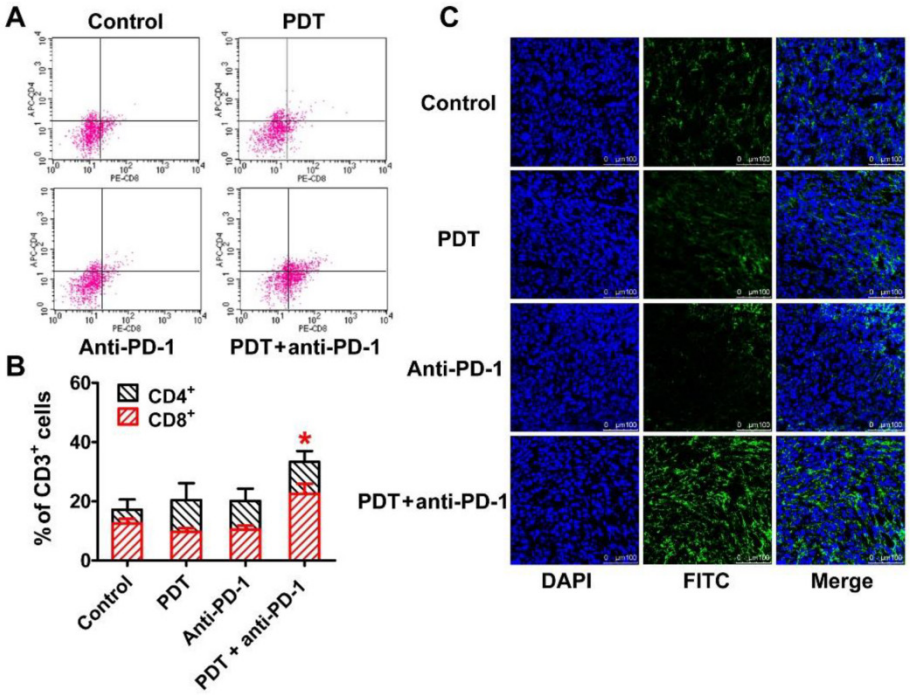

Figure 4. Recruitment induction of $CD8^+$ T lymphocytes in the second tumor by DSAB-HK PDT of the first tumor followed by PD-1 blockade. (A, B) Representative dot plots (A) and quantified $CD4^+$ or $CD8^+$ cells (B) by flow cytometric analyses of the single-cell suspension of the second tumor harvested from mice after different treatments as indicated. (C) Immunofluorescence staining of CD8α in the second tumor tissues from mice after different treatments. *, $P < 0.05$.

Taken together, these results demonstrated that PDT stimulation increased the recruitment and activation of DCs (serving as antigen-presenting cells) to facilitate the infiltration of cytotoxic T lymphocytes into the tumor. However, the function of T lymphocytes is negatively regulated by the expression of PD-1 [34]. PD-1 blockade using an anti-PD-1 antibody could prevent the inactivation of T lymphocytes rather than increasing their infiltration into tumors (**Figure 4**). Therefore, neither PDT only nor PD-1 blockade alone led to a sufficient number of activated cytotoxic T lymphocytes ($CD8^+$ T cells) within the tumor (**Figure 4**). In contrast, the combination of PDT and PD-1 blockade significantly inhibited the tumor growth by inducing both the T lymphocyte infiltration and activation within the tumor.

Specific targeting of DSAB-HK in lung metastasis

In the clinical setting, metastasis is major reason for tumor-related deaths. As metastasis and primary tumors generally co-exist, the ablation of primary tumors (e.g. by surgery) with concomitant destruction of distant metastases would be a useful strategy for effective tumor therapy. We hypothesized that DSAB-HK could be used for noninvasive imaging of primary tumors and also their metastatic lesions, and that under NIRF image-guidance, the tumors could be killed by subsequent PDT after light irradiation. In addition, the host immune system might be triggered after tumor PDT, thereby improving the anti-tumor efficacy of combination PDT and PD-1 blockade. To achieve this, we first investigated the targeting efficacy of DSAB-HK in a lung metastatic mouse model. For this, 4T1 tumor cells were stably transfected with firefly luciferase to generate the 4T1-fLuc cell line to allow the in vivo monitoring by BLI of the tumor cells after luciferin administration. A robust linear correlation between the 4T1-fLuc cell number and fLuc activity was observed ($R^2 = 0.9906$, $P < 0.0001$; **Figure S7**), suggesting the accuracy of in vivo BLI for monitoring cell proliferation. By day 10 after injection of 4T1-fLuc cells into the mice via the tail vein, lung metastases were successfully formed. We then injected DSAB-HK into the lung metastatic mouse model, and a notably higher NIRF signal in the chest area was observed for the DSAB-HK treated group as compared to that of the DSAB group from 1 to 8 h (**Figure 5A**). In addition, no evident DSAB-HK accumulation was observed in the lungs of normal mice (**Figure 5A**). To further confirm the specific localization of DSAB-HK to the metastatic lesions, the same mice were administered with luciferin and BLI was performed immediately after the NIRF imaging at 8 h postinjection of DSAB-HK. The mice in both the DSAB-HK and DSAB groups formed evident lung metastases as indicated by evident BLI signal in the lung areas (**Figure 5B**). However, a substantively higher NIRF signal was found in the chests of the DSAB-HK group as compared to that in the DSAB

group (**Figure 5B**). Immediately after in vivo imaging, the mice were sacrificed, and the lungs were disserted and imaged ex vivo. A marked uptake was also observed for DSAB-HK as compared with that of DSAB (**Figure 5C**). We next performed an ex vivo biodistribution study of DSAB-HK in lung metastatic and normal mice, as well as of DSAB in the lung metastatic mice. The mice were sacrificed and ex vivo imaged by the optical imaging system. A significantly higher light signal for DSAB-HK was observed in the lungs of the metastatic mice compared to that in the normal lungs, as well as to that of DSAB in the metastatic lungs ($P < 0.05$; **Figure 5D** and **E**). These results confirmed the specific in vivo targeting of DSAB-HK in the metastatic lesions. It should be noted that autofluorescent proteins (e.g., chlorophyll in the mouse diet) can be non-specifically excited during the process of NIRF imaging, which might create significant spontaneous background autofluorescence signals in the stomach [35].

DSAB-HK PDT and PD-1 blockade combination therapy in a mouse model bearing both subcutaneous and lung metastatic tumors

We next investigated the synergistic anti-tumor effect of DSAB-HK PDT and PD-1 blockade in the mouse model bearing both subcutaneous and lung metastatic tumors, which mimics the clinical situation of both primary tumor and tumor metastases to distant sites. The mice were inoculated subcutaneously with 4T1-fLuc tumor cells and injected with 4T1-fLuc cells through the tail vein (**Figure 6A**). After DSAB-HK administration, light irradiation (PDT) was conducted on either the subcutaneous tumor only or on both the subcutaneous and lung tumors (irradiating the mouse chests) (twice on days 1 and 5). An anti-PD-1 antibody was intravenously injected at 100 μg daily for three days (on days 2, 6, and 8), and BLI was performed longitudinally to monitor the growth of lung metastatic tumors. As the subcutaneous 4T1-fLuc tumor might also form lung metastases, we removed the subcutaneous tumors by surgery on the second day (on day 6) after the last PDT, and only observed the growth of lung metastases by BLI.

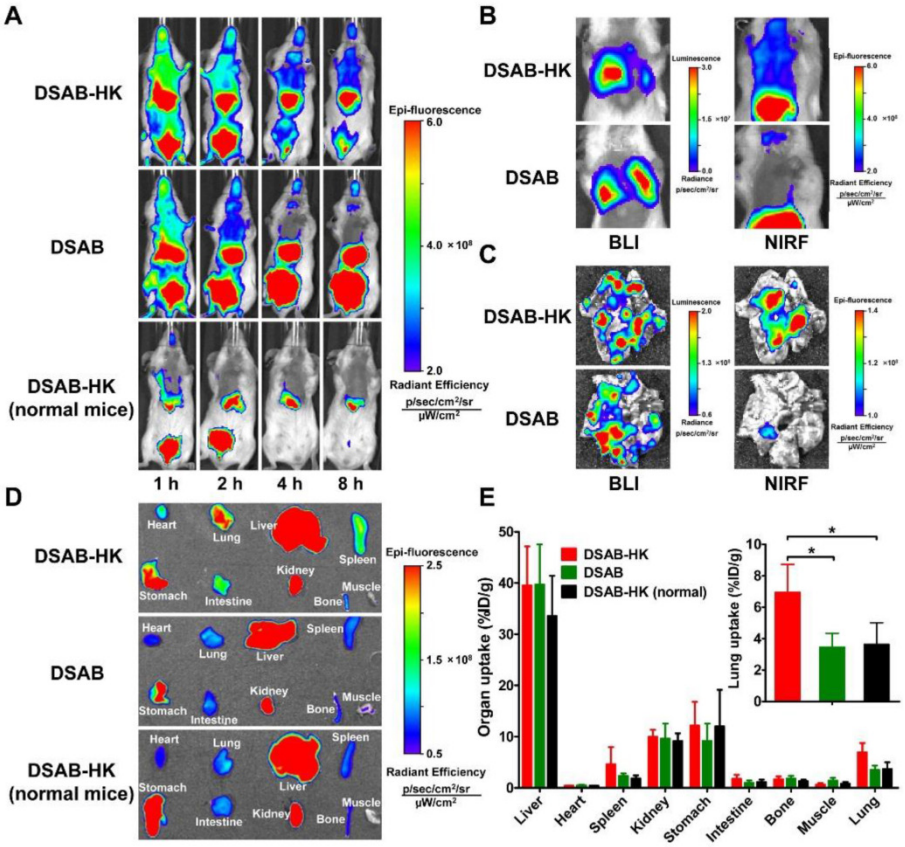

Figure 5. In vivo specific targeting of DSAB-HK in the lung metastatic 4T1-fLuc tumors. (A) In vivo NIRF imaging of lung metastatic mice or normal mice at 1, 2, 4, and 8 h after injection of DSAB-HK or DSAB. (B) In vivo BLI (left) and NIRF imaging (right) of mice bearing lung metastatic 4T1-fLuc tumors at 8 h after injection of DSAB-HK or DSAB. (C) Ex vivo BLI (left) and NIRF imaging (right) of the lungs dissected from the mice of (B). (D, E) Ex vivo NIRF imaging (D) and quantified probe uptake (E) of the major organs at 8 h postinjection of DSAB-HK or DSAB in lung metastatic or normal mice. Inset, quantified probe uptake in the lung. *, $P < 0.05$.

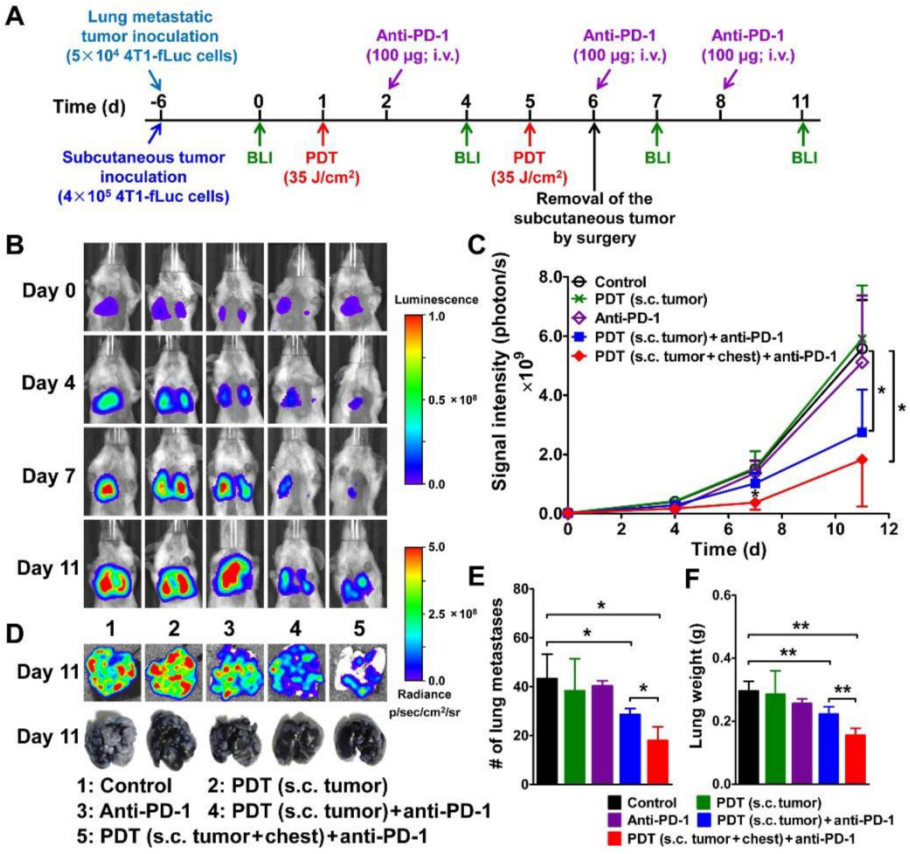

Figure 6. Significant growth inhibition of 4T1-fLuc lung metastasis treated with DSAB-HK PDT of the subcutaneous (s.c.) tumor or both the s.c. tumor and mouse chest (lung area) followed by PD-1 blockade as determined by BLI. (A) Scheme of DSAB-HK PDT and PD-1 blockade combination therapy, as well as the BLI schedule. (B) Serial bioluminescence images of 4T1-fLuc tumor-bearing mice after the indicated treatments. (C) Quantified bioluminescence signals from the lungs of (B). (D) Representative bioluminescence images of the lungs dissected from mice and photographs of India ink-filled lungs. (E, F) Counted averages of tumor metastatic lesions on the surfaces of India ink-filled lungs (E) and measured whole lung weights (F) immediately following dissection from mice. *, $P < 0.05$; **, $P < 0.01$.

Compared with the control, PDT only, and PD-1 blockade only groups, DSAB-HK PDT of the subcutaneous tumor plus PD-1 blockade significantly suppressed the growth of lung metastatic tumors on day 11 ($P < 0.05$; **Figure 6B** and **C**). A most effective effect on the suppression of tumor growth in the lungs was observed in DSAB-HK PDT group (both subcutaneous tumor and lung area) plus PD-1 blockade (**Figure 6B** and **C**). The in vivo BLI results were well validated using ex vivo BLI imaging of the lungs after dissection (**Figure 6D**). The lungs of the mice were also either filled with India ink to count the tumor lesions on the lung surface or directly weighed for the assessment of tumor growth in the whole lung. Compared with the control group, the lungs after DSAB-HK PDT (on subcutaneous tumors) along with PD-1 blockade showed remarkably reduced metastasis, as evidenced by the count of lung metastases on the lung surface ($P < 0.05$; **Figure 6D** and **E**) and the measurement of lung weight ($P < 0.01$; **Figure 6F**). The effect of DSAB-HK PDT + PD-1 blockade on the growth inhibition of lung metastatic tumors was further enhanced by PDT of both subcutaneous tumors and the lung areas of the mice (**Figure 6D**, **E**, and **F**).

In this proof-of-concept study, we demonstrated the synergistic effects of tumor-targeted PDT and immune checkpoint inhibition for inhibiting tumor growth and suppressing metastases in a 4T1 mouse breast cancer mouse model. Future studies to investigate this strategy in other tumor models and optimize of the therapeutic doses might be needed to further validate the synergistic effect of PDT and PD-1 blockade. In addition, although an effective therapeutic response was observed in this study, the tumor regression and metastasis inhibition were partial rather than complete. Several recent studies have suggested that optimal therapeutic results of immune checkpoint inhibition require combinatory blockade of both PD-1 and CTLA-4 [36, 37]. Therefore, further improvements in anti-tumor efficacy might be achieved by treatment combinations of PDT and immune checkpoint inhibitors targeting both the PD-1 and CTLA-4 pathways.

Conclusions

In this study, we have shown that a phthalocyanine dye-labeled NIRF probe DSAB-HK could specifically identify subcutaneous as well as lung metastatic

tumor lesions noninvasively by targeting integrin αvβ6 that is specifically expressed on the tumor cells surface. Upon light irritation, a remarkable PDT effect of DSAB-HK was observed both in vitro and in vivo. DSAB-HK-based PDT could significantly counter the challenge of the second tumors by promoting the maturation of DCs in the TDLN. The effectiveness of anti-tumor immunity triggered by DSAB-HK PDT could be significantly enhanced by combination with immune checkpoint inhibition of PD-1 blockade as evidenced by significantly increased recruitment of $CD8^+$ cytotoxic T lymphocytes to the tumor. In a dual subcutaneous tumor and metastatic mouse model, DSAB-HK PDT of the subcutaneous tumor in combination with PD-1 blockade significantly inhibited the growth of lung metastases. Our results demonstrated that tumor-targeted PDT using DSAB-HK offers an effective therapeutic benefit for treating primary tumors as well as metastases at distant sites through combination with checkpoint inhibition. The findings of this study might also be extended to combining PDT with other materials or photosensitizers or other tumor target-based specific PDTs with immune checkpoint inhibition for synergistic anti-tumor therapy.

Supplementary Material

Supplementary Methods, Figures S1-S7.
http://www.thno.org/v06p0627s1.pdf

Acknowledgements

This work was partially supported by the National Basic Research Program of China (973 program) (2013CB733802), the National Natural Science Foundation of China (81471712, 81222019, and 81420108019), the Beijing Natural Science Foundation (7132131), and the Beijing Nova Program (Z121107002512010).

Competing Interests

The authors have declared that no competing interest exists.

References

1. Mathers CD, Loncar D. Projections of global mortality and burden of disease from 2002 to 2030. PLoS Med. 2006; 3: e442.
2. Schroeder A, Heller DA, Winslow MM, et al. Treating metastatic cancer with nanotechnology. Nat Rev Cancer. 2012; 12: 39-50.
3. Steeg PS. Tumor metastasis: mechanistic insights and clinical challenges. Nat Med. 2006; 12: 895-904.
4. Gupta GP, Massague J. Cancer metastasis: building a framework. Cell. 2006; 127: 679-95.
5. Blattman JN, Greenberg PD. Cancer immunotherapy: a treatment for the masses. Science. 2004; 305: 200-5.
6. Mellman I, Coukos G, Dranoff G. Cancer immunotherapy comes of age. Nature. 2011; 480: 480-9.
7. Wherry EJ. T cell exhaustion. Nat Immunol. 2011; 12: 492-9.
8. Pardoll DM. The blockade of immune checkpoints in cancer immunotherapy. Nat Rev Cancer. 2012; 12: 252-64.
9. Hodi FS, O'Day SJ, McDermott DF, et al. Improved survival with ipilimumab in patients with metastatic melanoma. N Engl J Med. 2010; 363: 711-23.
10. Vanneman M, Dranoff G. Combining immunotherapy and targeted therapies in cancer treatment. Nat Rev Cancer. 2012; 12: 237-51.
11. Topalian SL, Hodi FS, Brahmer JR, et al. Safety, activity, and immune correlates of anti-PD-1 antibody in cancer. N Engl J Med. 2012; 366: 2443-54.
12. Hamid O, Robert C, Daud A, et al. Safety and tumor responses with lambrolizumab (anti-PD-1) in melanoma. N Engl J Med. 2013; 369: 134-44.
13. Yuan A, Wu J, Tang X, et al. Application of near-infrared dyes for tumor imaging, photothermal, and photodynamic therapies. J Pharm Sci. 2013; 102: 6-28.
14. Sato K, Nagaya T, Choyke PL, et al. Near infrared photoimmunotherapy in the treatment of pleural disseminated NSCLC: preclinical experience. Theranostics. 2015; 5: 698-709.
15. Sato K, Hanaoka H, Watanabe R, et al. Near infrared photoimmunotherapy in the treatment of disseminated peritoneal ovarian cancer. Mol Cancer Ther. 2015; 14: 141-50.
16. Mitsunaga M, Ogawa M, Kosaka N, et al. Cancer cell-selective in vivo near infrared photoimmunotherapy targeting specific membrane molecules. Nat Med. 2011; 17: 1685-91.
17. Nakajima T, Sano K, Choyke PL, et al. Improving the efficacy of Photoimmunotherapy (PIT) using a cocktail of antibody conjugates in a multiple antigen tumor model. Theranostics. 2013; 3: 357-65.
18. Gao D, Gao L, Zhang C, et al. A near-infrared phthalocyanine dye-labeled agent for integrin alphavbeta6-targeted theranostics of pancreatic cancer. Biomaterials. 2015; 53: 229-38.
19. van Duijnhoven FH, Aalbers RI, Rovers JP, et al. The immunological consequences of photodynamic treatment of cancer, a literature review. Immunobiology. 2003; 207: 105-13.
20. Castano AP, Mroz P, Hamblin MR. Photodynamic therapy and anti-tumour immunity. Nat Rev Cancer. 2006; 6: 535-45.
21. Liu Z, Yu Z, He W, et al. In-vitro internalization and in-vivo tumor uptake of anti-EGFR monoclonal antibody LA22 in A549 lung cancer cells and animal model. Cancer Biother Radiopharm. 2009; 24: 15-24.
22. Gao L, Liu H, Sun X, et al. Molecular imaging of post-Src-inhibition tumor signatures for guiding dasatinib combination therapy. J Nucl Med. 2016; 57: 321-326.
23. Liu Z, Sun X, Liu H, et al. Early assessment of tumor response to gefitinib treatment by noninvasive optical imaging of tumor vascular endothelial growth factor expression in animal models. J Nucl Med. 2014; 55: 818-23.
24. Zhang C, Gao L, Cai Y, et al. Inhibition of tumor growth and metastasis by photoimmunotherapy targeting tumor-associated macrophage in a sorafenib-resistant tumor model. Biomaterials. 2016; 84: 1-12.
25. Curran MA, Montalvo W, Yagita H, et al. PD-1 and CTLA-4 combination blockade expands infiltrating T cells and reduces regulatory T and myeloid cells within B16 melanoma tumors. Proc Natl Acad Sci U S A. 2010; 107: 4275-80.
26. Sun X, Gao D, Gao L, et al. Molecular imaging of tumor-infiltrating macrophages in a preclinical mouse model of breast cancer. Theranostics. 2015; 5: 597-608.
27. Liu Z, Liu H, Ma T, et al. Integrin αvβ6-targeted SPECT imaging for pancreatic cancer detection. J Nucl Med. 2014; 55: 989-94.
28. Bandyopadhyay A, Raghavan S. Defining the role of integrin αvβ6 in cancer. Curr Drug Targets. 2009; 10: 645-52.
29. Berchtold S, Muhl-Zurbes P, Heufler C, et al. Cloning, recombinant expression and biochemical characterization of the murine CD83 molecule which is specifically upregulated during dendritic cell maturation. FEBS Lett. 1999; 461: 211-6.
30. Wesa AK, Galy A. IL-1 beta induces dendritic cells to produce IL-12. Int Immunol. 2001; 13: 1053-61.
31. Waitz R, Solomon SB, Petre EN, et al. Potent induction of tumor immunity by combining tumor cryoablation with anti-CTLA-4 therapy. Cancer Res. 2012; 72: 430-9.
32. Wang C, Xu L, Liang C, et al. Immunological responses triggered by photothermal therapy with carbon nanotubes in combination with anti-CTLA-4 therapy to inhibit cancer metastasis. Adv Mater. 2014; 26: 8154-62.
33. Vanpouille-Box C, Diamond JM, Pilones KA, et al. TGFβ is a master regulator of radiation therapy-induced antitumor immunity. Cancer Res. 2015; 75: 2232-42.
34. Keir ME, Francisco LM, Sharpe AH. PD-1 and its ligands in T-cell immunity. Curr Opin Immunol. 2007; 19: 309-14.
35. Inoue Y, Izawa K, Kiryu S, et al. Diet and abdominal autofluorescence detected by in vivo fluorescence imaging of living mice. Mol Imaging. 2008; 7: 21-7.
36. Wolchok JD, Kluger H, Callahan MK, et al. Nivolumab plus ipilimumab in advanced melanoma. N Engl J Med. 2013; 369: 122-33.
37. Twyman-Saint Victor C, Rech AJ, Maity A, et al. Radiation and dual checkpoint blockade activate non-redundant immune mechanisms in cancer. Nature. 2015; 520: 373-7.